ISSN 1674-1056
http://cpb.iphy.ac.cn
http://iopscience.iop.org/cpb
中国物理 B
Chinese Physics
中国物理
Chinese Physics B

Nonlocal effect on resonant radiation force exerted on semiconductor coupled quantum well nanostructures

Jin-Ke Zhang(张金珂), Ting-Ting Zhang(张婷婷), Yu-Liang Zhang(张玉亮), Guang-Hui Wang(王光辉), Dong-Mei Deng(邓冬梅)

Citation: Chin. Phys. B . 2019, 28(6): 066803. **doi:** 10.1088/1674-1056/28/6/066803
Journal homepage: http://cpb.iphy.ac.cn; http://iopscience.iop.org/cpb

What follows is a list of articles you may be interested in

Tunable resonant radiation force exerted on semiconductor quantum well nanostructures:Nonlocal effects

Guang-Hui Wang(王光辉), Xiong-Shuo Yan(颜雄硕), Jin-Ke Zhang(张金珂)
Chin. Phys. B . 2017, 26(10): 106802. **doi:** 10.1088/1674-1056/26/10/106802

Efficiency droop suppression in GaN-based light-emitting diodes by chirped multiple quantum well structure at high current injection

Zhao Yu-Kun, Li Yu-Feng, Huang Ya-Ping, Wang Hong, Su Xi-Lin, Ding Wen, Yun Feng
Chin. Phys. B . 2015, 24(5): 056806. **doi:** 10.1088/1674-1056/24/5/056806

Effects of prestrained InGaN interlayer on the emission properties of InGaN/GaN multiple quantum wells in a laser diode structure

Cao Wen-Yu, He Yong-Fa, Chen Zhao, Yang Wei, Du Wei-Min, Hu Xiao-Dong
Chin. Phys. B . 2013, 22(7): 076803. **doi:** 10.1088/1674-1056/22/7/076803

Optically pumped GaN/AlGaN quantum well intersubband terahertz laser

Fu Ai-Bing, Hao Ming-Rui, Yang Yao, Shen Wen-Zhong, Liu Hui-Chun
Chin. Phys. B . 2013, 22(2): 026803. **doi:** 10.1088/1674-1056/22/2/026803

Nonlocal effect on resonant radiation force exerted on semiconductor coupled quantum well nanostructures*

Jin-Ke Zhang(张金珂)[1,2], Ting-Ting Zhang(张婷婷)[1,2], Yu-Liang Zhang(张玉亮)[1,2], Guang-Hui Wang(王光辉)[1,2,†], and Dong-Mei Deng(邓冬梅)[1,2]

[1] *Guangzhou Key Laboratory for Special Fiber Photonic Devices, South China Normal University, Guangzhou* 510006, *China*
[2] *Guangdong Provincial Key Laboratory of Nanophotonic Functional Materials and Devices, South China Normal University, Guangzhou* 510006, *China*

(Received 24 January 2019; revised manuscript received 28 March 2019; published online 8 May 2019)

Based on the microscopic nonlocal optical response theory, the resonant radiation force exerted on a semiconductor-coupled quantum well nanostructure (CQWN), induced by the nonlocal interaction between lasers and electrons in conduction bands, is investigated for two different polarized states. The numerical results show that the spatial nonlocality of optical response can cause a radiation shift (blue-shift) for the spectrum of the resonant radiation force, which is dependent on the CQWN width ratio, the barrier height, and polarized states sensitively. It is also confirmed that the resonant radiation force is steerable by the incident and polarized directions of incident light. This work may provide an advantageous method for detecting internal quantum properties of nanostructures, and open novel and raising possibilities for optical manipulation of nano-objects using laser-induced radiation force.

Keywords: nonlocal effect, resonant radiation force, coupled quantum well

PACS: 68.65.Fg, 45.20.da, 11.10.Lm **DOI:** 10.1088/1674-1056/28/6/066803

1. Introduction

Utilizing optical force to alter the motion of micrometre-sized particles[1] and neutral atoms[2] could have potential applications in the manipulation of microscopic particles and of individual atom. Therefore, the optical force and optical manipulation of nano-objects have been attracting extensive interests and have been successfully applied in various fields such as plasmonic nanoparticles, quantum dots, biology, *etc.*[3–11] For example, Nieto-Vesperinas *et al.*[5] had announced the study of the optical force on a small particle with both electric and magnetic response, and clarified the origin and significance of the electric–magnetic dipolar interaction force, which is related with the angular distribution of the extinction cross section and of scattered light.

Recently, the nonlocal optical effects in semiconductor and metal nanostructures have been drawing more and more attention.[12–20] The so-called nonlocal optical response is that the polarization at a spatial point is induced by the applied optical fields not only at the same point, but also at other positions within the extent of the relevant wave function of electrons. Therefore, when we take the nonlocal optical response into account, susceptibility tensors and dielectric permittivity would be more complex. These pioneering works of spatial nonlocality in semiconductor materials have developed into two successful research aspects: nanostructures[21] and metamaterials.[22] For instance, Mortensen[23] had found some important nonlocal effects in metamaterials and Batke *et al.*[24] demonstrated a strong nonlocal interaction of two-dimensional (2D) magnetoplasmon resonance with harmonics of the cyclotron resonance in AlGaAs/GaAs heterostructures. Moreover, there are also a great deal of interests in nonlocal optical effects for mesoscopic systems, resulting in the development of nonlocal theory and nonlocal optical properties in plasmon and semiconductor nanostructures.[25–28] The nonlocal optical response of metal nanostructures with arbitrary shape had been investigated and the particular importance of nonlocal effects in apex structures had been indicated by McMahon *et al.*[20] Furthermore, Kosionis *et al.*[29] had also taken nonlocal effects into consideration in the research on optical effects in quantum-dot/metal–nanoparticle hybrid systems. As far as we know, the spatial nonlocal effects on optical force have not been clarified. It is reasonable to believe that the spatial nonlocal effects may have an important influence on the optical force exerted on nanodevices. The physical motive of our paper is to demonstrate and explain the optical force exerted on a coupled semiconductor quantum well nanostructure (CQWN) from the resonant intersubband transitions for two different polarized states under spatial nonlocal effects.

This paper is organized as follows. In Section 2, a basic theoretical framework for optical force applied on a CQWN with two kinds of polarized states is presented by taking the

*Project supported by the Natural Science Foundation of Guangdong Province, China (Grant Nos. 2016A030313439 and 2018A030313480), GDUPS (2017), the Key Program of the Natural Science Foundation of Guangdong Province, China (Grant No. 2017B030311003), and the Science and Technology Program of Guangzhou City, China (Grant No. 201707010403).

†Corresponding author. E-mail: wanggh@scnu.edu.en

© 2019 Chinese Physical Society and IOP Publishing Ltd

spatial nonlocality of optical response into account. Section 3 is dedicated to the results and discussions for AlGaAs/GaAs CQWN. And finally, our conclusions are given in Section 4.

2. Theoretical framework for optical force on a CQWN with nonlocal response

In what follows, let us consider that a monochromatic plane wave with an incident angle θ and an angular frequency ω in the cases of p- and s-polarized states, is incident on a CQWN confined in the z direction, as shown in Fig. 1. In general, the Lorentz force acting on an object induced by an electromagnetic field is described as[30]

$$\boldsymbol{F}(t)=\int_V[\rho(\boldsymbol{r},t)\boldsymbol{E}(\boldsymbol{r},t)+\boldsymbol{j}(\boldsymbol{r},t)\times\boldsymbol{B}(\boldsymbol{r},t)]\,\mathrm{d}\boldsymbol{r}, \tag{1}$$

where $\boldsymbol{E}(\boldsymbol{r},t)$ and $\boldsymbol{B}(\boldsymbol{r},t)$ are the electric and magnetic fields, respectively. $\rho(\boldsymbol{r},t)$ is the charge density, and $\boldsymbol{j}(\boldsymbol{r},t)$ is the current density. V is the volume of the force body. The charge density can be written as $\rho(\boldsymbol{r},t)=-\nabla\cdot\boldsymbol{P}(\boldsymbol{r},t)$, where $\boldsymbol{P}(\boldsymbol{r},t)$ is the induced polarization intensity.

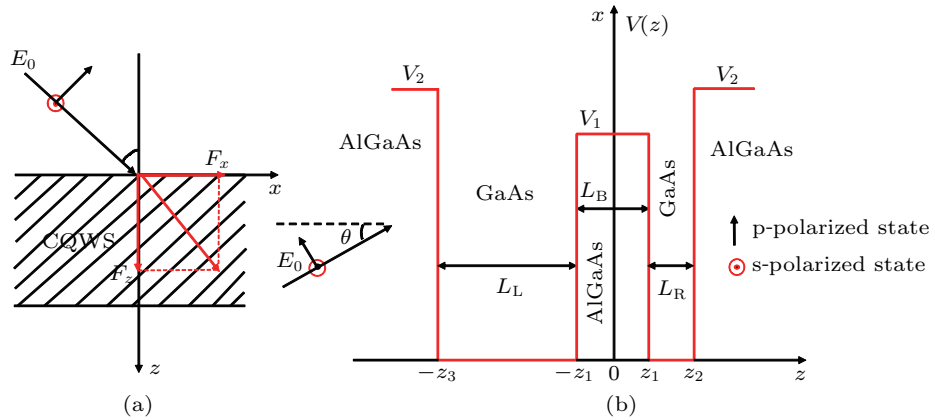


Fig. 1. (a) The schematic diagrams of radiation forces acting on a CQWN confined in the z direction, where F_x and F_z denote the x and z components of the radiation force induced by a monochromatic plane wave with p- or s-polarized state, respectively. (b) The schematic diagrams of the CQWN, where L_L, L_B, and L_R denote the left well, mid-barrier, and right well widths, V_1 and V_2 denote the mid-barrier and outer barrier height, respectively. The signs ↑ and ⊙ denote polarization direction of p- and s-polarized light waves, respectively.

For time-harmonic electromagnetic fields, we have

$$\begin{aligned}\boldsymbol{E}(\boldsymbol{r},t)&=\mathrm{Re}\{\boldsymbol{E}(\boldsymbol{r},\omega)\exp(-\mathrm{i}\omega t)\},\\ \boldsymbol{B}(\boldsymbol{r},t)&=\mathrm{Re}\{\boldsymbol{B}(\boldsymbol{r},\omega)\exp(-\mathrm{i}\omega t)\},\\ \boldsymbol{P}(\boldsymbol{r},t)&=\mathrm{Re}\{\boldsymbol{P}(\boldsymbol{r},\omega)\exp(-\mathrm{i}\omega t)\},\end{aligned}$$

where $\boldsymbol{E}(\boldsymbol{r},\omega)$, $\boldsymbol{B}(\boldsymbol{r},\omega)$, and $\boldsymbol{P}(\boldsymbol{r},\omega)$ are complex functions of position and frequency. Re denotes the real part. The time-averaged force in the case of time-harmonic electromagnetic fields is derived as[8]

$$\langle\boldsymbol{F}\rangle(\omega)=\frac{1}{2}\mathrm{Re}\left\{\int_V\mathrm{d}\boldsymbol{r}\nabla\boldsymbol{E}(\boldsymbol{r},\omega)^*\cdot\boldsymbol{P}(\boldsymbol{r},\omega)\right\}, \tag{2}$$

where * denotes the complex conjugate. Under the nonlocal linear response, the resonant part of the induced polarization is described as

$$\boldsymbol{P}(\boldsymbol{r},\omega)=\varepsilon_0\int_V\overleftrightarrow{\chi}(\boldsymbol{r},\boldsymbol{r}';\omega)\cdot E(\boldsymbol{r}',\omega)\,\mathrm{d}\boldsymbol{r}', \tag{3}$$

where $\overleftrightarrow{\chi}(\boldsymbol{r},\boldsymbol{r}';\omega)$ is the nonlocal susceptibility tensor. Due to the system with translational invariance in the x direction and confinement in the z direction, the complex electric field $\boldsymbol{E}(\boldsymbol{r},\omega)$ and polarization $\boldsymbol{P}(\boldsymbol{r},\omega)$ can be assumed to have the forms $\boldsymbol{E}(\boldsymbol{r},\omega)=\widetilde{\boldsymbol{E}}(z;\omega)\exp(\mathrm{i}k_x x)$ and $\boldsymbol{P}(\boldsymbol{r},\omega)=\widetilde{\boldsymbol{P}}(z;\omega)\exp(\mathrm{i}k_x x)$, where k_x stands for the wave number in the x direction.

In the following, let us consider the AlGaAs/GaAs CQWN restricted in the z direction, as shown in Fig. 1. Based on the effective mass approximation, the Schrödinger equation for electrons in CQWN can be written as

$$\left[-\frac{\hbar^2}{2m^*}\nabla^2+V(z)\right]\psi_{n,q}(\boldsymbol{r})=E_{n,k}\psi_{n,q}(\boldsymbol{r}), \tag{4}$$

with the confinement potential $V(z)$

$$V(z)=\begin{cases}V_2, & z<-z_3,\\ 0, & -z_3<z<-z_1,\\ V_1, & -z_1<z<z_1,\\ 0, & z_1<z<z_2,\\ V_2, & z>z_2,\end{cases} \tag{5}$$

where z represents the confinement direction of the CQWN; V_1 and V_2 denote the mid-barrier and outer barrier height, respectively; $\hbar$ is Planck constant; m^* is the effective mass of an electron in the conduction band; $E_{n,q}$ and $\psi_{n,q}(\boldsymbol{r})$ denote the eigenenergies and eigenfunctions of the CQWN system, respectively. Due to the translational invariance in the xy plane and the confinement in the z direction of the system, $\psi_{n,q}(\boldsymbol{r})$ and $E_{n,q}$ can be written as

$$\psi_{n,q}(\boldsymbol{r})=\frac{1}{2\pi}\mathrm{e}^{\mathrm{i}\boldsymbol{q}_\parallel\cdot r_\parallel}\varphi_n(z), \tag{6}$$

and

$$E_{n,q} = \varepsilon_n + \frac{\hbar^2}{2m^*}|\boldsymbol{q}_{||}|^2, \tag{7}$$

here, $\boldsymbol{q}_{||}$ and $\boldsymbol{r}_{||}$ are electronic wave vector and position vector in the xy plane. The solutions of one-dimensional Schrödinger equation $H_0\varphi_n(z) = \varepsilon_n\varphi_n(z)$, with $H_0 = -(\hbar^2/2m^*)(\mathrm{d}^2/\mathrm{d}z^2) + V(z)$, are $\varphi_n(z)$ and ε_n, which are named the envelope wave functions and the corresponding transverse energies of the n-th subband, respectively.

For the finite-depth CQWN, the transverse energy eigenvalue ε_n and the corresponding electronic envelope wave function $\varphi_n(z)$ in the CQWN can be expressed as

$$\varphi_n(z) = \begin{cases} a_n \exp(k_1 z), & z < -z_3, \\ b_{1n}\sin(k_2 z) + b_{2n}\cos(k_2 z), & -z_3 < z < -z_1, \\ c_{1n}\exp(k_3 z) + c_{2n}\exp(-k_3 z), & -z_1 < z < z_1, \\ d_{1n}\sin(k_2 z) + d_{2n}\cos(k_2 z), & z_1 < z < z_2, \\ e_n \exp(-k_1 z), & z > z_2, \end{cases} \tag{8}$$

where $k_1 = \sqrt{2m^*(V_2 - \varepsilon_n)}/\hbar$, $k_2 = \sqrt{2m^*\varepsilon_n}/\hbar$, and $k_3 = \sqrt{2m^*(V_1 - \varepsilon_n)}/\hbar$. We can obtained the coefficients a_n, b_{1n}, b_{2n}, c_{1n}, c_{2n}, d_{1n}, d_{2n}, e_n, and the transverse energy eigenvalue ε_n by using the continuity of envelope wave function at the boundaries.

By substituting Eq. (3) into Maxwell's equations, we can derive the integral–differential equation for the self-consistent complex electric field $\boldsymbol{E}(\boldsymbol{r},\omega)$ under the nonlocal linear optical response,[15] *viz.*

$$\overleftrightarrow{\Lambda}(\omega)\cdot\widetilde{\boldsymbol{E}}(z;\omega) = -\frac{\omega^2}{c^2}\int \mathrm{d}z'\overleftrightarrow{\chi}(z,z';\omega)\cdot\widetilde{\boldsymbol{E}}(z';\omega), \tag{9}$$

where the tensorial operator

$$\overleftrightarrow{\Lambda}(\omega) = \overleftrightarrow{I}\left[\frac{\omega^2}{c^2}\varepsilon^{\mathrm{B}}(\omega) - k_x^2 + \frac{\partial^2}{\partial z^2}\right] - \left(\mathrm{i}k_x\hat{e}_x + \hat{e}_z\frac{\partial}{\partial z}\right)\left(\mathrm{i}k_x\hat{e}_x + \hat{e}_z\frac{\partial}{\partial z}\right).$$

Here c is the speed of light in vacuum. $\overleftrightarrow{I}$ denotes the unit tensor. $\hat{e}_x$ and $\hat{e}_z$ denote unit vectors in the x and z directions, respectively. $\varepsilon^{\mathrm{B}}(\omega)$ is the relative dielectric constant of the background medium. By the one-body density matrix method,[15] the components of the linear polarization, $\widetilde{\boldsymbol{P}}(z,\omega)$, for the two-level CQWN model can be obtained in the low-temperature ($T \to 0$) and long wavelength approximation ($k_x \to 0$) limits as follows:

$$\widetilde{P}_j(z,\omega) = -\frac{e^2}{2\pi\hbar^2\omega^2}\frac{(\varepsilon_{\mathrm{F}} - \varepsilon_1)^2 N_j\Psi(z)}{\hbar\omega - \varepsilon_{21} + \mathrm{i}\hbar\Gamma_0}, \quad (j = x,y), \tag{10}$$

$$\widetilde{P}_z(z,\omega) = \frac{e^2}{4\pi m^*\omega^2}\frac{(\varepsilon_1 - \varepsilon_{\mathrm{F}})N_z\zeta(z)}{\hbar\omega - \varepsilon_{21} + \mathrm{i}\hbar\Gamma_0}, \tag{11}$$

where

$$N_j \equiv \int_{-\infty}^{\infty}\Psi(z)\widetilde{E}_j(z;\omega)\mathrm{d}z,$$

$$N_z \equiv \int_{-\infty}^{\infty}\zeta(z)\widetilde{E}_z(z;\omega)\mathrm{d}z,$$

and $\Psi(z) = \varphi_1(z)\varphi_2(z)$; $\zeta(z) = \varphi_1(z)\mathrm{d}\varphi_2(z)/\mathrm{d}z - \varphi_2(z)\mathrm{d}\varphi_1(z)/\mathrm{d}z$, $\varepsilon_{21} = \varepsilon_2 - \varepsilon_1$; e is the electron charge; Γ is the off-diagonal relaxation rate; $\varepsilon_{\mathrm{F}} = \varepsilon_1 + \pi N_{\mathrm{s}}\hbar^2/m^*$ is the Fermi energy of the CQWN system, where N_{s} is the donor surface concentration.

By the Green's function method,[15,21] one can solve the components of the microscopic electric field ($\widetilde{E}_y$ for s-polarized state, $\widetilde{E}_x$ and $\widetilde{E}_z$ for p-polarized state) from Eq. (9) as follows:

$$\widetilde{E}_y(z;\omega) = \widetilde{E}_{0y}(z;\omega) + \frac{\alpha N_y}{2\mathrm{i}k_\perp}\int_{-\infty}^{\infty}\mathrm{e}^{\mathrm{i}k_\perp|z-z'|}\Psi(z')\mathrm{d}z', \tag{12}$$

$$\widetilde{E}_x(z;\omega) = \widetilde{E}_{0x}(z;\omega) + \alpha N_x\int_{-\infty}^{\infty}G_{xx}(z,z';\omega)\Psi(z')\mathrm{d}z' + \beta N_z\int_{-\infty}^{\infty}G_{xz}(z,z';\omega)\zeta(z')\mathrm{d}z', \tag{13}$$

$$\widetilde{E}_z(z;\omega) = \widetilde{E}_{0z}(z;\omega) + \alpha N_x\int_{-\infty}^{\infty}G_{zx}(z,z';\omega)\Psi(z')\mathrm{d}z' + \beta N_z\int_{0}^{L}G_{zz}(z,z';\omega)\zeta(z')\mathrm{d}z', \tag{14}$$

where $\widetilde{\boldsymbol{E}}_0(z;\omega) = \widetilde{\boldsymbol{E}}_0\exp(\mathrm{i}k_\perp z)$ is the incident field, and $k_\perp = (\varepsilon_{\mathrm{b}}\omega^2/c^2 - k_x^2)^{1/2}$ is the wave number in the z direction. In addition, $\alpha = \mu_0\mathrm{e}^2(\varepsilon_{\mathrm{F}} - \varepsilon_1)^2/(2\pi\hbar^2\Lambda)$, and $\beta = \mu_0\mathrm{e}^2(\varepsilon_{\mathrm{F}} - \varepsilon_1)/(4\pi m^*\Lambda)$, where $\Lambda = \hbar\omega - \varepsilon_{21} + \mathrm{i}\hbar\Gamma_0$. $G_{ij}(z,z';\omega)$ $(i,j = x,z)$ are the elements of the tensorial Green's function $\overleftrightarrow{G}(z,z';\omega)$ of the CQWN system[15]

$$\overleftrightarrow{G}(z,z';\omega) = \frac{k_x c^2\mathrm{e}^{\mathrm{i}k_\perp|z-z'|}}{2\mathrm{i}\varepsilon_{\mathrm{b}}\omega^2}\begin{pmatrix} k_\perp/k_x & \mathrm{sgn}(z'-z) \\ \mathrm{sgn}(z'-z) & k_x/k_\perp \end{pmatrix} + \frac{\delta(z'-z)c^2}{\varepsilon_{\mathrm{b}}\omega^2}\hat{\boldsymbol{e}}_z\hat{\boldsymbol{e}}_z, \tag{15}$$

where $\mathrm{sgn}(z)$ is the usual sign function.

By multiplying both sides of Eqs. (12)–(14) by $\Psi(z)$ and $\zeta(z)$, respectively, then integrating the three equations over z across the CQWN, one can obtain

$$N_y = \widetilde{S}_y/(1 - \alpha M_{yy}), \tag{16}$$

$$N_x = \frac{\widetilde{S}_x(1 - \beta M_{zz}) + \beta\widetilde{S}_z M_{xz}}{(1 - \alpha M_{xx})(1 - \beta M_{zz}) - \alpha\beta M_{xz}M_{zx}}, \tag{17}$$

$$N_z = \frac{\widetilde{S}_z(1 - \alpha M_{xx}) + \alpha\widetilde{S}_x M_{zx}}{(1 - \alpha M_{xx})(1 - \beta M_{zz}) - \alpha\beta M_{xz}M_{zx}}, \tag{18}$$

where

$$M_{xx} = \int\int_{-\infty}^{\infty}\Psi(z)G_{xx}(z,z';\omega)\Psi(z')\mathrm{d}z\mathrm{d}z',$$

$$M_{yy} = 1/(2\mathrm{i}k_\perp)\int\int_{-\infty}^{\infty}\Psi(z)\mathrm{e}^{\mathrm{i}k_\perp|z-z'|}\Psi(z')\mathrm{d}z\mathrm{d}z',$$

$$M_{xz} = -M_{zx} = \int\int_{-\infty}^{\infty}\Psi(z)G_{xz}(z,z';\omega)\zeta(z')\mathrm{d}z\mathrm{d}z',$$

$$M_{zz} = \int\int_{-\infty}^{\infty}\zeta(z)G_{zz}(z,z';\omega)\zeta(z')\mathrm{d}z\mathrm{d}z',$$

$$\widetilde{S}_j = \int_{-\infty}^{\infty} \widetilde{E}_{0j}(z;\omega)\Psi(z)\,\mathrm{d}z, \quad (j=x,y),$$
$$\widetilde{S}_z = \int_{-\infty}^{\infty} \widetilde{E}_{0z}(z;\omega)\zeta(z)\,\mathrm{d}z.$$

Note that, for the following analyses, equations (16)–(18) can be written in vectorial form by the rotating wave approximation[21]

$$\overleftrightarrow{D}\cdot\widetilde{\boldsymbol{N}} = \widetilde{\boldsymbol{S}}, \tag{19}$$

where $\overleftrightarrow{D}$ is a 3×3 diagonal matrix with the elements given below[21]

$$D_{xx} = \hbar\omega - \varepsilon_{21} + \mathrm{i}\hbar\Gamma_0 + hM_{xx},$$
$$D_{yy} = \hbar\omega - \varepsilon_{21} + \mathrm{i}\hbar\Gamma_0 + hM_{yy},$$
$$D_{zz} = \hbar\omega - \varepsilon_{21} + \mathrm{i}\hbar\Gamma_0 + tM_{zz}.$$

The vectors $\widetilde{\boldsymbol{S}} = (\widetilde{S}_x, \widetilde{S}_y, \widetilde{S}_z)$ and $\widetilde{\boldsymbol{N}} = g(\widetilde{N}_x, \widetilde{N}_y, \widetilde{N}_z)$, where $g = 1/(\hbar\omega - \varepsilon_{21} + \mathrm{i}\hbar\Gamma_0)$, $h = -\mu_0\,\mathrm{e}^2(\varepsilon_\mathrm{F} - \varepsilon_1)^2/2\pi\hbar^2$, and $t = \mu_0\,\mathrm{e}^2(\varepsilon_\mathrm{F} - \varepsilon_1)/4\pi m^*$.

However, if we only take local optical response into account, the complex electric field $\boldsymbol{E}(\boldsymbol{r},\omega)$ and polarization $\boldsymbol{P}(\boldsymbol{r},\omega)$ can be written as

$$\boldsymbol{E}(\boldsymbol{r},\omega) = \boldsymbol{E}_0 \exp[\mathrm{i}(k_x x + k_z z)], \tag{20}$$
$$\boldsymbol{P}(\boldsymbol{r},\omega) = \varepsilon_0 \overleftrightarrow{\chi}(\omega)\cdot E(\boldsymbol{r},\omega), \tag{21}$$

where k_x and k_z stand for the wave number in the x and z direction in the CQWN, respectively; $\overleftrightarrow{\chi}(\omega)$ is the local linear susceptibility tensor, whose elements $\chi_{xx}(\omega) = \chi_{yy}(\omega) = 0$, $\chi_{zz}(\omega) = e^2 m^*(\varepsilon_\mathrm{F} - \varepsilon_1)|\mu_{21}|^2/[\pi\varepsilon_0 L\hbar^2(\hbar\omega - \varepsilon_{21} + \mathrm{i}\hbar\Gamma_0)]$, here $\mu_{21} = \int_{-\infty}^{\infty}\varphi_2^*(z)z\varphi_1(z)\,\mathrm{d}z$ and L is the total width of the CQWN.

By substituting Eq. (20) and Eq. (21) into Eq. (2), we can obtain the numerical solution of the resonant radiation force exerted on the CQWN in the case of the local optical response.

3. Results and discussion

To discuss the optical force exerted on the CQWN, we take the spatial nonlocality of optical response into account in detail. Some parameters used in the following calculation are adopted as:[12,14] $m^* = 0.067m_0$ (m_0 is the mass of a free electron), $N_\mathrm{s} = 10^{11}$ cm^{-2}, $\varepsilon_\mathrm{b} = 13.1$, and the mid-barrier width $L_\mathrm{B} = 1$ nm. The incident intensity is assumed to be 0.05 W/cm^2.

In Section 2, based on Eqs. (10)–(14), we can solve the components of the microscopic electric field $\boldsymbol{E}(z;\omega)$ and induced polarization $\boldsymbol{P}(z;\omega)$ by the Green's function method[15,21] and one-body density matrix method,[15] respectively. Substituting these components into Eq. (2), we can obtain the numerical solution of the resonant radiation force, then analyze the resonant radiation force spectra.

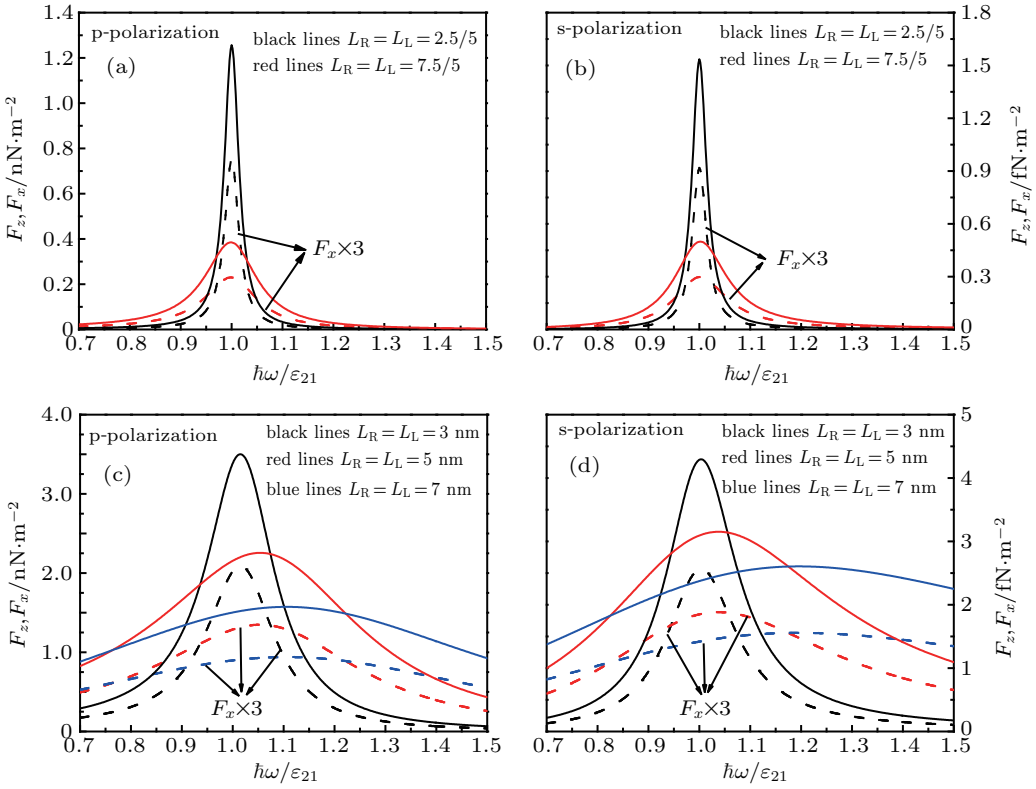


Fig. 2. Resonant radiation force spectra (F_x dashed lines; F_z solid lines) in the two cases of p- and s-polarization for two different width ratios: $L_\mathrm{R}/L_\mathrm{L} = 2.5/5$ (black lines), $L_\mathrm{R}/L_\mathrm{L} = 7.5/5$ (red lines) [panels (a) and (b)], and for the three different CQWN widths: $L_\mathrm{R} = L_\mathrm{L} = 3$ nm (black lines), $L_\mathrm{R} = L_\mathrm{L} = 5$ nm (red lines), and $L_\mathrm{R} = L_\mathrm{L} = 7$ nm (blue lines) [panels (c) and (d)]. The mid-barrier width $L_\mathrm{B} = 1$ nm, and the barrier height $V_1 = V_2 = 2.0$ meV, $\hbar\Gamma_0 = 4.7$ meV.

In Figs. 2(a) and 2(b), the resonant radiation force is shown as a function of the normalized photon energy $\hbar\omega/\varepsilon_{21}$ for asymmetric CQWN of two different width ratios between the right well width L_R and the left well width L_L: $L_R/L_L = 2.5/5$ (black line), $L_R/L_L = 7.5/5$ (red line) with the left well width $L_L = 5$ nm in two cases: (a) p-polarization and (b) s-polarization with the incident angle $\theta = 45°$, and the barrier height $V_1 = V_2 = 2.0$ meV. For the sake of contrast, we also plot the resonant radiation force of the symmetric CQWN for three different widths: $L_R = L_L = 3$ nm (black lines), $L_R = L_L = 5$ nm (red lines), and $L_R = L_L = 7$ nm (blue lines) with the same condition in Figs. 2(c) and 2(d). F_x and F_z denote the x and z components of the radiation force, respectively, where F_x has been amplified three times so as to contrast with F_z. From Fig. 2, one can find easily some important properties of resonant radiation force spectra: (i) The resonance peak does not occur at $\hbar\omega/\varepsilon_{21} = 1$, whereas it has a deviation relative to the energy separation ε_{21} more or less, namely, the resonance peak position occurs at $\hbar\omega/\varepsilon_{21} = 1+\Delta$, where Δ is called a radiation shift, which is attributed to the nonlocal optical response in the CQWN system. The magnitude of the radiation shift is dependent on the structure parameters and symmetry of the CQWN. When the CQWN is asymmetric, the radiation shift is not evident, that is, the position of the resonance peak of radiation force occurs at $\hbar\omega/\varepsilon_{21} \approx 1$, as shown in Figs. 2(a) and 2(b). When the CQWN is symmetric, however, the radiation shift is evident, and the wider the symmetric CQWN is, the larger the radiation shift will be, as shown in Figs. 2(c) and 2(d). It is because that, compared with asymmetric CQWN, the wave functions of symmetric CQWN would be broadened more due to stronger coupling effects between two wells of symmetric CQWN, which leads the characteristic response scale of electrons to increase. (ii) F_z is evidently larger than F_x in the same polarized state. This is because the quantum-size effect plays an important role in the z direction, which induces the increase of the intensity of electric polarization, due to the charged particles are confined in the z direction of the system.

In order to contrast the difference of the resonant radiation force under local and nonlocal response, we also plot the resonant radiation force spectra for local and nonlocal cases in p-polarization in Fig. 3. From Fig. 3, we can find that the nonlocality of optical response has an important influence on the resonant radiation force spectra. Obviously, the resonance peak of F_x and F_z has an evident blue-shift under nonlocal response, compared with those under local response with same conditions for p-polarized state. Furthermore, the amplitudes of F_x and F_z under nonlocal response are larger than those under local response, respectively. In addition, for s-polarized state, both F_x and F_z are equal to zero under local response due to the y component of polarization $\boldsymbol{P}$ is equal to zero in dipole approximation. However, they are not equal to zero under nonlocal response. The radiation shift of the resonant radiation force spectra due to the nonlocality of optical response is also demonstrated by Eq. (19). From Eq. (19) we can easily see that the resonance structures of the optical force spectra are determined by the roots of $\det|\overleftrightarrow{D}| = 0$. According to the expressions of the diagonal matrix elements D_{xx}, D_{yy}, and D_{zz}, it is obvious that the resonance peak does not occur at $\hbar\omega = \varepsilon_{21}$, but has a shift relative to the level interval ε_{21}, which is attributed to the contributions from the real part of the terms hM_{xx}, hM_{yy}, tM_{zz}, respectively.

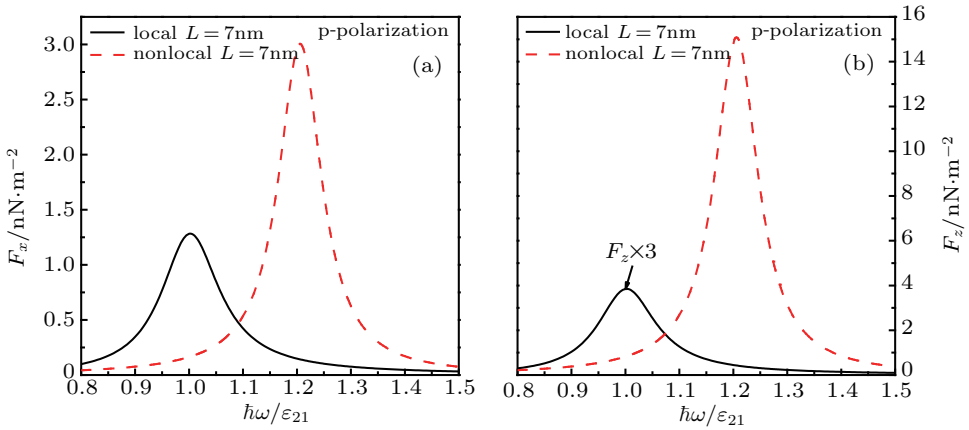


Fig. 3. Under local (solid lines) and nonlocal (dashed lines) response, the resonant radiation force spectra (F_x and F_z) in p-polarization for the well width: $L_R = L_L = 7$ nm. The mid-barrier width $L_B = 1$ nm, and the barrier height $V_1 = V_2 = 2.0$ meV. $\hbar\Gamma_0 = 0.47$ meV.

To see how the well-width ratio and the polarized state influence the resonant radiation force spectra, we plot the maximum radiation force (F_x and F_z) at resonance in Fig. 4 and the position of the resonance peak ($\hbar\omega/\varepsilon_{21}$) in Fig. 5 *versus* the well-width ratio L_R/L_L in the two cases of p- and s-polarizations, respectively. The black solid, red dashed, and blue dotted lines correspond to the barrier height ratios $V_1/V_2 = 0.4$, 0.7, and 1.0, respectively, with $L_L = 4$ nm and $V_2 = 2.0$ meV. In Figs. 4 and 5, it is evident that both the maximum radiation force and the position of the resonance peak

are closely relevant to the structure parameters of the CQWN, and the changing trend of F_x and F_z *versus* the well width ratio L_R/L_L is consistent essentially for p-polarization and s-polarization. From Fig. 4, we can see that with the increase of the well width ratio L_R/L_L, the maximum resonant radiation force decreases at first and then rises; when $L_R/L_L = 1$, that is, when the CQWN becomes symmetric, it attains a peak value. The CQWN degenerates to a single quantum well when $L_R/L_L = 0$, and the resonant radiation force is maximal at this point. When $L_R/L_L > 3.0$, the resonant radiation force does not increase with further increasing the CQWN width. When the well width ratio value L_R/L_L is in the approximate range from 1.5 to 1.8, a relative minimal resonant radiation force can be obtained. Furthermore, for a fixed CQWN width ratio, the resonant radiation force becomes smaller and smaller with the increase of the mid-barrier height V_1, when the width ratio L_R/L_L is in the range from 0.5 to 2.0. All the properties manifest that the resonant radiation force can be modulated by designing the structure parameters of CQWN.

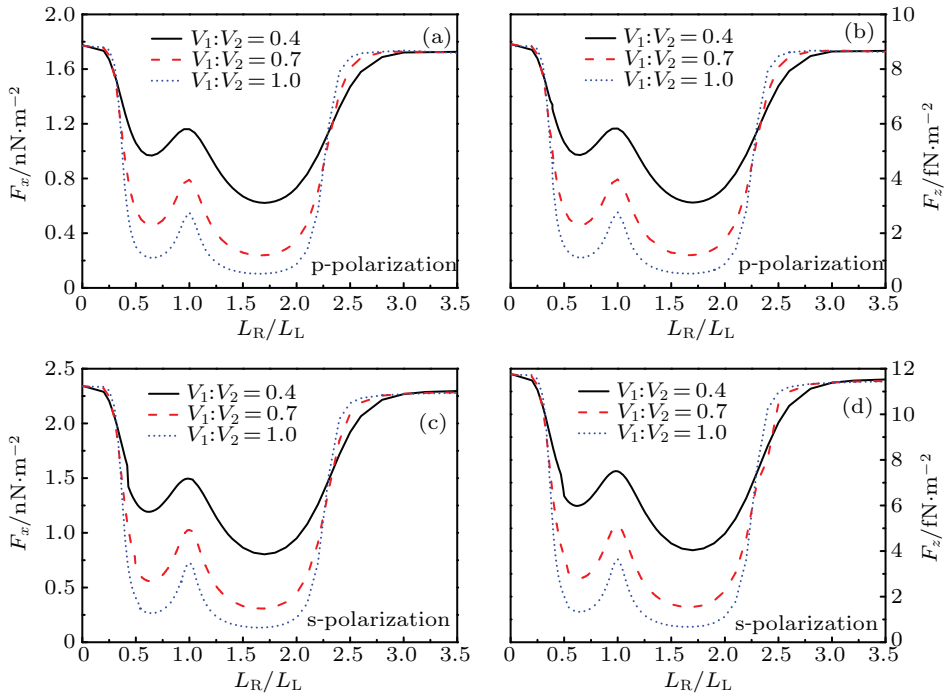


Fig. 4. The maximum resonant radiation force (F_x and F_z) *versus* the well-width ratio L_R/L_L in the two cases of p- and s-polarizations for $V_1/V_2 = 0.4$ (black solid line), 0.7 (red dashed line), 1.0 (blue dotted line) respectively, with the left well width $L_L = 4$ nm, and the outer barrier height $V_2 = 2.0$ meV, $\hbar\Gamma_0 = 4.7$ meV.

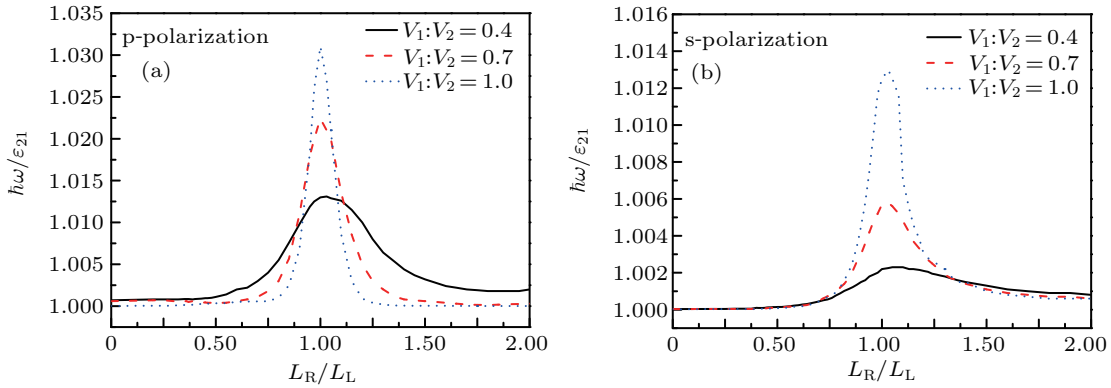


Fig. 5. The resonant peak position of optical force spectra, normalized by energy-level interval ε_{21}, *versus* the well width ratio L_R/L_L with the $V_1/V_2 = 0.4$ (black solid lines), 0.7 (red dash lines), 1.0 (blue dot lines) in the two cases of p-polarization and s-polarization, respectively, with the left well width $L_L = 4$ nm, and the outer barrier height $V_2 = 2.0$ meV, $\hbar\Gamma_0 = 4.7$ meV.

The well width ratio L_R/L_L is an important factor in influencing the position of resonance peak of the optical force spectra, as shown in Fig. 5. It is worth noting that the position of resonance peak would deviate from the energy interval ε_{21} due to the nonlocal interaction between electrons and laser fields. As the well width ratio L_R/L_L increases, the deviation of the resonance peak position is more and more evident; when $L_R/L_L = 1$, the deviation attains to a peak value, and then it decreases gradually. In other words, the radiation shift of optical force at resonance in symmetric CQWN is larger than

that in asymmetric CQWN generally. The reason is that, compared with asymmetric CQWN, the wave functions of symmetric CQWN would be broadened more due to stronger coupling effects between two wells of symmetric CQWN, which leads the characteristic response scale of electrons to increase. In addition, the barrier height also has influence on the radiation shift of the position of resonance peak of the optical force spectra in the two cases of p-polarization and s-polarization. It increases with the increase of mid-barrier height V_1, and is larger in the p-polarized state.

The change of maximum resonant radiation force (F_x and F_z) with the barrier height ratio V_1/V_2 is shown in Fig. 6 for three different well width ratios: $L_R/L_L = 2.5/5$ (black solid line), $L_R/L_L = 5/5$ (red dash line), $L_R/L_L = 7.5/5$ (blue dotted line) in the two cases of p-polarization [(a) and (b)] and s-polarization [(c) and (d)]. We can see clearly in Fig. 6 that the maximum resonant radiation forces (F_x and F_z) decrease gradually with the barrier height ratio V_1/V_2 increasing at first, and then tending to remain stable. It is because that the coupling effect would be weaken with the mid-barrier height increasing. In addition, for a fixed barrier height ratio V_1/V_2, the change of maximum resonant radiation force (F_x and F_z) with the well width ratio L_R/L_L is also in agreement with those shown in Fig. 3.

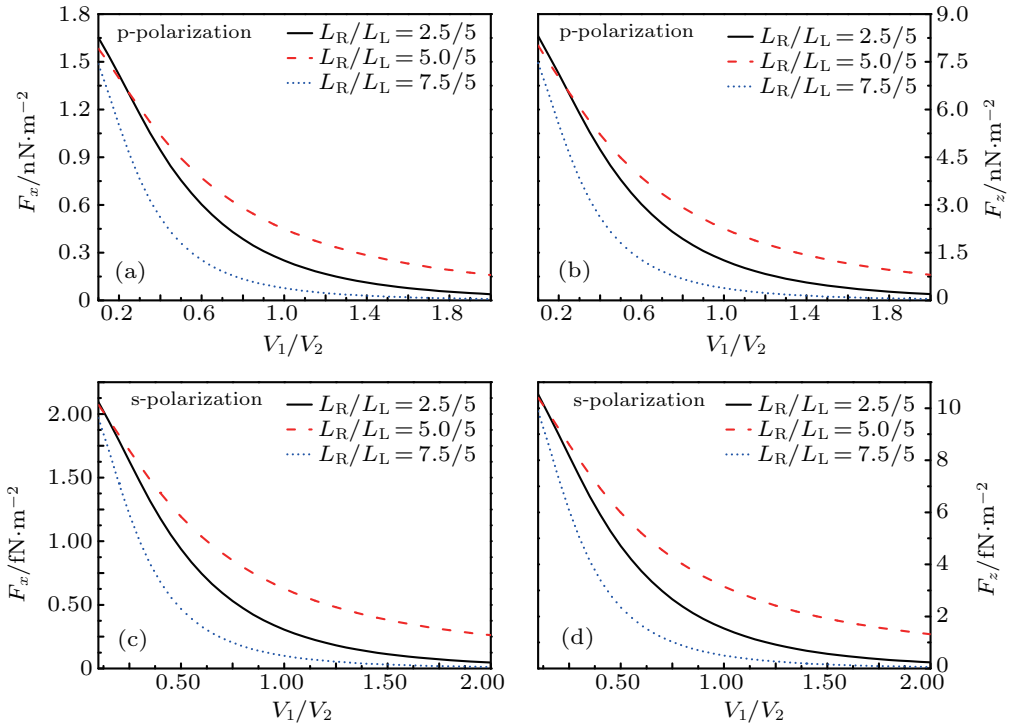


Fig. 6. The change of maximum resonant radiation force (F_x and F_z) *versus* the barrier height ratio V_1/V_2 for three different well width ratios: $L_R/L_L = 2.5/5, 5/5, 7.5/5$ in the two cases of p-polarization [(a) and (b)] and s-polarization [(c) and (d)], respectively, with the left well width $L_L = 5$ nm, and the outer barrier height $V_2 = 2.0$ meV, $\hbar\Gamma_0 = 4.7$ meV.

In Fig. 7, we show the maximum resonant force (F_x and F_z) *versus* the incident angle θ in the two cases of p-polarization [(a) and (b)], and s-polarization [(c) and (d)] for three different well-width ratios, respectively. We note that the maximum resonant radiation forces for the p-polarized state are much larger than those for the s-polarized state, except the case of $\theta = 0$. This is because there is a quantum-size effect for the p-polarized state, while it hardly works for the s-polarized state. Furthermore, we can see clearly that the incident angle has an evident influence on F_x and F_z. For p-polarized state, as the incident angle θ increases, it is obvious that both F_x and F_z increase in Figs. 7(a) and 7(b). This is because with θ increasing the z component of the incident field increases, causing an increase of the z component of the polarization $\widetilde{\boldsymbol{P}}(z,\omega)$ in the CQWN, and the quantum-size effect plays an important role in the z direction. When $\theta = 0°$, which means that the incident light is perpendicularly incident on the CQWN, and the electronic polarization parallels to the x direction, as a result that F_z at resonance is very small because the quantum-size effect have not any influence in this direction. When $\theta = 90°$, that is, the incident light is horizontally incident on the CQWN, the electronic polarization direction is completely parallel to the z direction, which leads to F_x and F_z at resonance to be maximum on account of the quantum-size effects. For the s-polarized state, we can see that F_z decreases and F_x increases with the incident angle θ increasing in Figs. 7(c) and 7(d). The reason for this is that the z component of wave vector will decrease and the x component will increase with the increase of incident angle, respectively. These properties make the CQWN a good candidate for optical manipulation of nano-objects using laser-induced radiation force.

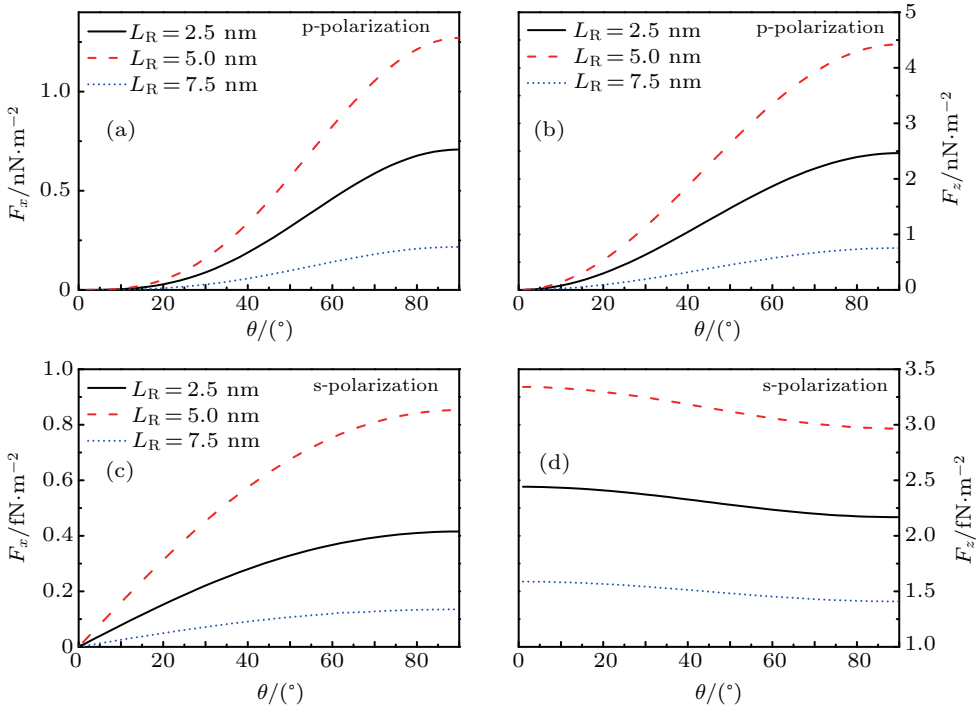


Fig. 7. Maximum resonant radiation force (F_x and F_z) *versus* the incident angle θ in the two cases of p-polarization [(a) and (b)], and s-polarization [(c) and (d)] for three different well-width ratios, respectively, with the left well width $L_L = 5$ nm, and the barrier height $V_1 = V_2 = 2.0$ meV, $\hbar\Gamma_0 = 4.7$ meV.

4. Conclusion

In this paper, we have theoretically investigated the nonlocal effects on optical force exerted on the AlGaAs/GaAs CQWN from the resonant intersubband transitions for two kinds of polarized states. We have shown that there exists a blue-shift of radiation force spectra at resonance caused by the spatial nonlocality of optical response, and with well width increasing, the radiation shift increases for symmetric CQWN, while it is more evident and larger than those for asymmetric CQWN. Moreover, it is also demonstrated that the resonant radiation force is controlled by the CQWN width ratio, the barrier height ratio, the polarized and incident directions of incident light. The designable CQWN provides a more advantageous way to obtain the suitable optical resonant radiation force. These properties have potential applications in detecting internal quantum properties inside nanostructures, and can open novel and exalting possibilities for the characterization, assembly and optical control of nano-objects.

References

[1] Ashkin A 1970 *Phys. Rev. Lett.* **24** 156
[2] Ashkin A 1970 *Phys. Rev. Lett.* **25** 1321
[3] Mandal S, Serey X and Erickson D 2010 *Nano. Lett.* **10** 99
[4] Righini M, Ghenuche P, Cherukulappurath S, Myroshnychenko V, García de Abajo F J and Quidant R 2009 *Nano. Lett.* **9** 3387
[5] Nieto-Vesperinas M, Sáenz J J, Gómez-Medina R and Chantada L 2010 *Opt. Express* **18** 11428
[6] Jauffred L, Richardson A C and Oddershede L B 2008 *Nano. Lett.* **8** 3376
[7] Chen Y F, Serey X, Sarkar R, Chen P and Erickson D 2012 *Nano. Lett.* **12** 1633
[8] Chaumet P C and Nietovesperinas M 2000 *Opt. Lett.* **25** 1065
[9] Maragò O M, Jones P H, Gucciardi P G, Volpe G and Ferrari A C 2013 *Nat. Nanotechnol.* **8** 807
[10] Cho S H, Lee J Y, Han J K and Cho B I 2010 *Ultrasound. Med. Biol.* **36** 202
[11] Li Y and Hu Y J 2013 *Chin. Phys. B* **22** 034206
[12] Wang G H, Guo Q, Wu L J and Yang X B 2007 *Phys. Rev. B* **75** 205337
[13] Wang G H, Yan X S and Zhang J K 2017 *Chin. Phys. B* **26** 106802
[14] Wang C Y and Wang G H 2014 *Chin. Phys. B* **23** 127103
[15] Liu A and Keller O 1995 *Phys. Scr.* **52** 116
[16] Chang R and Leung P T 2006 *Phys. Rev. B* **73** 125438
[17] Zhang X M, Xiao J J and Zhang Q 2014 *Chin. Phys. B* **23** 017302
[18] Lu J H and Wang G H 2016 *Chin. Phys. B* **25** 117804
[19] Teperik T V, Nordlander P, Aizpurua J and Borisov A G 2013 *Phys. Rev. Lett.* **110** 263901
[20] Mcmahon J M, Gray S K and Schatz G C 2009 *Phys. Rev. Lett.* **103** 097403
[21] Cho K 2003 *Optical Response of Nanostructures: Microscopic Nonlocal Theory* (Berlin: Springer-Verlag) pp. 1–32
[22] Belov P A, Marques R, Maslovski S I, Nefedov I S, Silveirinha M, Simovski C R and Tretyakov S A 2002 *Phys. Rev. B* **673** 181
[23] Mortensen N A, Raza S, Wubs M, Sondergaard T and Bozhevolnyi S I 2014 *Nat. Commun.* **5** 3809
[24] Batke E, Heitmann D and Tu C W 1986 *Phys. Rev. B* **34** 6951
[25] Raza S, Bozhevolnyi S I, Wubs M and Mortensen N A 2015 *J. Phys: Condens. Matter* **27** 183204
[26] Castaldi G, Galdi V, Alu A and Engheta N 2011 *Phys. Rev. Lett.* **108** 063902
[27] Wurtz G A, Pollard R, Hendren W, Wiederrecht G P, Gosztola D J, Podolskiy V A and Zayats A V 2011 *Nat. Nanotechnol.* **6** 107
[28] Luo Y, Fernande-zdominguez A I, Wiener A, Maier S A and Pendry J B 2013 *Phys. Rev. Lett.* **111** 093901
[29] Kosionis S G, Terzis A F, Yannopapas V and Paspalakis E 2014 *J. Phys. Chem. C* **116** 23663
[30] Jackson J D 1999 *Classical Electrodynamics* (New York: Willey) p. 3